JOURNAL OF GEOPHYSICAL RESEARCH, VOL. 91, NO. B7, PAGES 7343–7358, JUNE 10, 1986

Observations and Modeling of Seafloor Microseisms

S. C. WEBB AND C. S. COX

Scripps Institution of Oceanography, University of California, San Diego, La Jolla

The seismic noise level on the deep seafloor has been essentially unknown at periods longer than 10 s and poorly known at shorter periods. We present data obtained with two new types of seafloor instrumentation: a differential pressure gauge and an antenna which measures a horizontal component of the electric field. The electric field is closely related to the horizontal ground motion. The observed spectra can be divided into three frequency bands. At periods longer than 40 s surface gravity waves produce velocity and pressure fluctuations which are felt at the deep seabed and dominate other sources. This signal is expected to be uniform throughout the ocean basins and will make detecting small seismic waves at periods longer than 40 s difficult. At periods between 10 and 40 s the spectrum is much quieter and may approach the background observed at quiet land stations. The pressure signal in this band may be at least partially caused by very low frequency acoustic waves in the atmosphere. The electric field spectrum is much noisier, suggesting that horizontal motions may be larger than vertical motions. At periods slightly shorter than 10 s the pressure spectrum rises sharply 45 dB into the microseism peak. Many studies of microseisms have established a clear relationship between the ocean surface gravity wave field and microseisms. We have found close agreement between the theory of microseism generation and observations obtained while a small storm moved over a seafloor instrument. The microseism spectrum evolved in concert with the changing wind wave field. We found that plausible estimates of the directionality of the wind wave field as a function of frequency could be derived from the microseism observations. The structure of the microseism peak in frequency is also related to the properties of surface waves trapped in the upper layers of sediment. Our calculations of the forcing of microseisms by a distributed pressure field at the surface elucidate this relationship and allow a partial determination of sediment structure at an instrument site from the microseism observations.

INTRODUCTION

There is a need for seafloor-based seismograph stations because there are large areas of the earth's surface which are ocean covered and distant from islands. While extensive programs of short-period ocean bottom seismology have been established for more than 20 years, long-period instruments are much more difficult to deploy on the seafloor, and the level of seismic noise at the deep seafloor is essentially unknown at periods longer that 10 s and poorly known at shorter periods. Long-period instruments require precise leveling and a firm foundation which is lacking at oceanic sites. We have developed two new types of seafloor instrumentations which circumvent these problems and provide useful, although indirect, measurements of seafloor seismic noise: a differential pressure gauge and an antenna which is used to measure one component of the electric field.

In this paper we describe the results of the three experiments with two emphases: first, to describe the spectra of seafloor noise observed with these transducers and, second, to explain the physical processes involved and model the amplitude of the noise. *Webb and Cox* [1984] provide a short discussion of these same experiments.

Our observations span a broad range of frequencies from a fraction of a millihertz to a few hertz. We find that the observations can be divided into three frequency bands with different sources dominating seafloor noise in each band. Locations on the deep seafloor are very noisy at frequencies below 0.03 Hz; we infer from our pressure fluctuation measurements that the effects of long-period surface gravity waves will often overwhelm seismic sources. The hydrodynamic filtering of the ocean removes the effects of these waves at higher frequencies, and the spectrum of noise from deep sea sites may approach most land sites in a band from 0.03 to 0.1 Hz.

The prominent "microseism" peak is apparent in our observations at frequencies above 0.1 Hz. The microseism peak is commonly observed in spectra of ground motion from land seismometer stations. The source of this noise has long been identified with the nonlinear interaction of surface gravity waves at sea, [*Longuet-Higgins,* 1950], but seafloor observations with seismometers of long enough period to resolve fully the microseism peak are rare. *Latham and Sutton* [1966] and *Latham and Nowroozi* [1968] provide the groundwork for this paper. These authors investigated the relationship of wind and waves to the microseism peak. *Adair et al.* [1984] provide a comparison of ocean bottom seismometer observations of the microseism peak with observations from a seismometer in a hole drilled into the seafloor. *Prothero and Schaecher* [1984] describe a recent effort to make long-period seafloor seismometer observations. Other ocean bottom seismometer observations have been limited to periods shorter than a few seconds; *Brocher and Iwatake* [1982], *Bradner et al.* [1965], *Bradner and Dodds* [1964], and *McGrath* [1976] investigated sources and levels of seafloor noise.

Our measurements show very dramatically the relationship between the structure of the microseism peak and both the local wind wave field and the structure of the sediment underneath the instrument site. The first rela-

Paper number 5B5540.
0148-2227/86/005B-5540$5.00

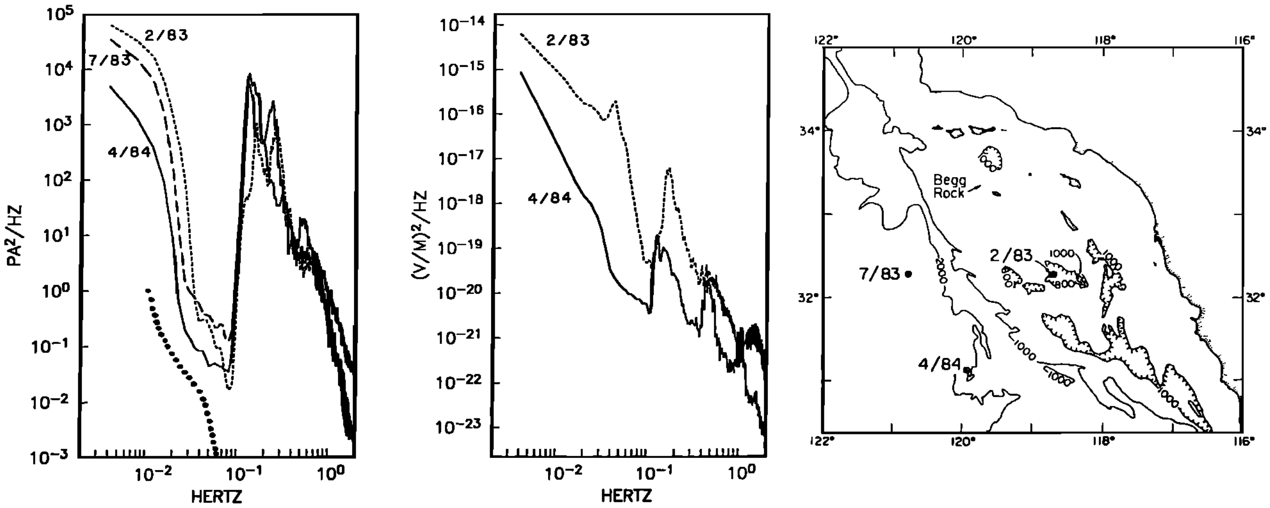

Fig. 1. Power spectra of (left) pressure fluctuations and (middle) electric field fluctuations from the February 1983, July 1983, and April 1984 experiments. An estimate of the pressure spectrum of long-period acoustic waves in the atmosphere is plotted with the pressure measurements (dotted line). (Right) The locations of these experiments are shown, labeled with the month and year. Wave height observations were made at a location near Begg Rock. Isobaths are marked with the depth in fathoms (1 fathom = 1.829 m)

tionship is demonstrated by measurements made while a small storm passed above of the instrument on the seafloor. The second connection is better demonstrated in the later two experiments when the effects of local forcing are not as important.

Spectra measured by the differential pressure gauge show much smaller levels for typical seafloor pressure noise at periods longer than 10 s than has been previously reported in the literature [*Nichols*, 1981; *Latham et al.*, 1967]. Conventional hydrophone systems are noisy at long-periods [*Cox et al.*, 1984].

Horizontal particle motion has been inferred from the voltage appearing across the antenna on the seafloor. The motion of the seafloor and seawater through the geomagnetic field induces an electric field. The electric field measurements are unique in that they represent an average of the motion over the length of the antenna (600-m). This property may lessen the influence of local inhomogeneities of the underlying sediments on the measurements. Mechanical coupling between the antenna and the sediments should be very strong, so that the antenna should follow ground motion closely.

The instruments were deployed during three experiments off of southern California in water from 1.5 to 3.8 km deep. Power spectra calculated from measurements obtained during these experiments are very similar in structure (Figure 1). Both the electric field and pressure fluctuation spectra show much more energy at low frequencies (below 0.04 Hz) and at high frequencies (above 0.1 Hz) than in the band between. In this paper we describe first the low-frequency band (0.001-0.04 Hz), then the intermediate band (0.04-0.1 Hz), and finally the high-frequency band (0.1-2 Hz) which contains the microseism peak. The pressure and electric field observations are augmented with wave height and wind velocity observations. In the last part of this paper we have produced extensive numerical calculations to explain the relationship of the structure of the microseism peak to the surface gravity wave field and to local earth structure.

In the next section of this paper we describe the transducers and their properties. In particular, we show that the electric field is related to the local particle velocities above and below the seafloor.

INSTRUMENTATION

We have made observations of the seafloor pressure and electric field fluctuations at three sites off southern California, as marked in Figure 1. The three experiments took place in February 1983, July 1983, and April 1984 (see Table 1). During the February experiment an instrument was placed in a 1500-m deep basin near San Clemente Island. The other two experiments were sited in deep water (>3500 m) beyond the Patton escarpment, which is the edge of the southern California borderland. Both pressure and electric field were not necessarily recorded continuously; Table 1 provides a description of sampling frequencies and times for each experiment. R. Seymour has kindly provided us with wave records from a buoy near Begg Rock. Short records of wave height were available 4 times a day during each of the experiments.

The pressure transducer is described in detail by *Cox, et al.* [1984]. The transducer is based on a small silicon strain gauge that measures the pressure difference between the ocean and an oil-filled rigid reference chamber. A capillary leak allows reequilibration of the pressure in the reference chamber with the ocean on a time scale of a hundred seconds. The instrumental noise appears to be well below the signal over the entire frequency band described in this paper. The gauge is calibrated to within 10%. At very long-periods, temperature fluctuations can effect the measurements, and we attribute a steep rise in the pressure spectrum at periods longer than 500 s to temperature fluctuations changing the pressure within the reference chamber.

The electric field instruments must be extraordinarily sensitive to measure the small electric fields associated with seismic motions. On land the electrical signals

TABLE 1. Experiment Locations and Dates

Begins		Ends		Location		Depth m	Wind m/s	Sampling Rate, Hz	Notes
Date	Time	Date	Time	Latitude N	Longitude W				
Feb. 1, 1983	1438	Feb.3, 1985	7016	32°18'	118°42'	1646	5–25	4 or 32	1,2,3,4
July 23, 1983	1214	July 27, 1983	1000	32°18'	120°44'	3847	5–10	4 or 32	1,4,5
April 15,1984	1903	April 25,1984	0517	31°15'	119°57'	3695	9–13	0.5 or 4	1,6

Notes: 1, 120°W meridian time. 2, There were two parallel antennas, 100 m and 600 m in length; both were tangled, and the effective lengths were 67 m and 351 m; the two channels were coherent at all frequencies. 3, The pressure channel was not sampled until Feb. 2, 1983, at 0823. 4, There are occasional gaps in the first 12 hours of data. 5, Both electric field channels failed. 6, There were two electric field antennas, one was 600 m long; the other was 1 m long.

from the fluctuations of the magnetosphere are much larger than the ground motion signal over the entire frequency band relevant to seismologists, but at the seafloor the magnetospheric fields are attenuated. The fields are reduced through the ocean exponentially with the skin depth $d_s = (2/\omega\mu\sigma)^{1/2}$ defining the scale length (ω is the frequency, μ the magnetic permeability, and σ the ocean conductivity). The magnetospheric noise reaches an instrument under 1500 m of seawater at periods longer than about 25 s. In the deeper water of the April experiment (3500 m+) the magnetospheric noise is not apparent at periods shorter than 35 s.

One horizontal component of the electric field is inferred from the voltage appearing across a long antenna lying on the seafloor. The antenna is an insulated wire several hundred meters in length. Electrical contact with the seawater is made through a carefully constructed pair of silver-silver chloride electrodes, one on the far end of the antenna, the other laid on the seafloor near the instrument package. The voltage appearing across the antenna is measured with an amplifier in which the $1/f$ noise is removed by chopper modulation of the signal. This signal and the pressure data are digitized and sampled at 0.5, 4, or 32 Hz and recorded on a high-density digital tape recorder for retrieval on recovery of the instrument.

Observations made with a pair of electrodes placed together on the seafloor are our best estimate of the instrumental noise on the electric field observations. In Figure 2 a spectrum of the voltage between a pair of closely spaced electrodes on the seafloor has been converted to an equivalent electric field noise spectrum for a 600-m antenna (dotted line). We have also plotted the range observed in electric field spectra measured with a 600-m antenna during the same experiment (solid lines). The lowest spectral densities observed lie well above the predicted noise spectrum, suggesting that we are observing principally geophysical signals.

The amplifiers in these instruments are calibrated to within a few percent, but there are much larger uncertainties in the effective length of the antennas. An antenna is stretched along the bottom by flying it down to the bottom as the instrument is slowly lowered behind a moving ship. The antenna became tangled during the February deployment, but acoustic transponders on each end of the antenna allowed a determination of the distance between the electrodes (351 m) to an accuracy of perhaps 5%. The April deployment appeared to be completely successful, but we have no way of determining if the antenna was stretched to the full 600-m length. *Cox et al.* [1970] note that additional errors can arise if the antenna is not colinear beyond the simple shortening of the distance between the electrodes.

We have previously examined the theory of the induction of electromagnetic fields by seismic waves [*Webb and Cox*, 1982]. A voltage is induced in the antenna when the antenna is moved through the geomagnetic field or by any electric field that is present in the seawater. Seismic waves induce an electric field in the seawater by moving the seawater through the geomagnetic field. The efficiency of this induction process depends on the induction number $I = \mu\sigma c^2/\omega$, where μ is the magnetic permeability, σ is the conductivity of seawater, c is the phase velocity, and ω is the frequency of the waves. This number is

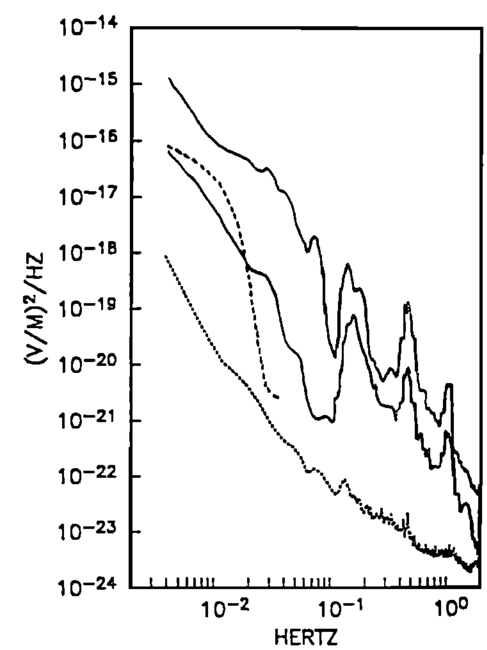

Fig. 2. The envelope of 10 estimates of the power spectrum of the electric field from 4096-s data sections obtained every 9.1 hours during the April 1984 experiment. The dashed line is an estimate of the contribution to the electric field fluctuations by surface gravity waves. The dotted line is an estimate of instrumental noise.

very large for seismic surface waves with periods longer than 10 s, but becomes small for slowly propagating surface waves with periods shorter than 1 s. For large induction number the electric field in the seawater approaches

$$\mathbf{E}_w = -\mathbf{u}_w \times \mathbf{F} \tag{1}$$

where $\mathbf{u}_w$ is the local particle velocity in the seawater and $\mathbf{F}$ is the geomagnetic induction. The horizontal component of the electric field is usually only slightly effected by the change in conductivity at the seafloor, as the sediment is not sufficiently conducting over a great enough depth that the motions in the sediment can efficiently induce electric fields.

Long-period surface gravity waves are also efficient generators of electric field, since they produce only very small motions of the seafloor; equation (1) is an adequate estimate of the measurable field. Seismic waves move the seafloor on which the antenna lies, and so the net voltage measured across the antenna is approximately

$$V = [(\mathbf{u}_s - \mathbf{a}\, \mathbf{u}_w) \times \mathbf{F}] \cdot \mathbf{l} \tag{2}$$

where $\mathbf{u}_s$ is the velocity of the seafloor, $\mathbf{u}_w$ the water velocity just above the seafloor, and $\mathbf{l}$ is a vector representing the length and direction of the antenna. To represent the varying efficiency of the induction process, we use the complex variable $\mathbf{a}$ with a magnitude which varies from 0 to 1 depending on the induction number. Love waves propagating under a flat bottomed ocean do not move the seawater; the voltage induced in the antenna is simply $V = [\mathbf{u}_s \times \mathbf{F}] \cdot \mathbf{l}$. This expression is also valid for Rayleigh waves of small induction number (high frequency).

In this paper we divide the voltage observed by the antenna length to describe the component of the electric field in the direction of the antenna. For Love waves,

$$\mathbf{E} = \mathbf{u}_s \times \mathbf{F} \tag{3}$$

Rayleigh waves are efficient generators of electric fields at periods longer than 1 s, and $\mathbf{a} \sim 1$ in equation (2). Throughout this paper we will use the approximation

$$\mathbf{E} = \Delta\mathbf{u} \times \mathbf{F} \tag{4}$$

to describe the electric field in the moving reference frame of the antenna. Here $\Delta\mathbf{u}$ is the jump in the particle velocity across the seafloor interface. The normal component of the particle velocity is continuous across any interface, so $\Delta\mathbf{u}$ is a horizontal vector. At periods longer than 20 s the seafloor velocity in Rayleigh waves is large compared to the water velocity and the electric field is a direct measure of seafloor motion. At microseism frequencies the two velocities are comparable.

Long-Period Gravity Waves

Typical seafloor pressure spectra observed during the three experiments are plotted in Figure 1. The minimum in spectral energy between 0.03 and 0.1 Hz is readily apparent in all three spectra. Above 0.1 Hz the spectra rise sharply into the microseism peak. Below 0.03 Hz the effects of long-period surface gravity waves become dominant.

The amplitude of the pressure fluctuation at the seafloor is related to the pressure fluctuation at a level surface just below sealevel (p_0) in the surface gravity waves by

$$p_b = \frac{p_0}{\cosh(kh)} \tag{5}$$

where k is the wave number of the surface gravity wave and h is the water depth.

The pressure fluctuations are hydrodynamically low pass filtered by the ocean. The cutoff wave number occurs at smaller wave number and lower frequency in a deeper ocean. The July 1983 and April 1984 spectra show a lower-frequency roll off than the February 1983 spectrum because the water was shallower at the latter site.

Extrapolating the pressure spectra observed at the seafloor to the sea surface, we find spectral levels between 10^4 and 5×10^5 (see *Webb*, [1984] for details). The surface spectra are fairly featureless and in agreement with the observations of *Snodgrass et al.* [1966]. The measurements of *Filloux* [1980] of bottom pressure are also in rough agreement.

Surface gravity waves also induce an electric field (see equation (1)). The spectrum of electric field fluctuations induced by long-period surface gravity waves can be predicted from the bottom pressure spectrum if some assumption about the directionality of the wave field is made; we assume isotropy. The dashed line in Figure 2 is an estimate of the contribution to the electric field from surface gravity waves; the range of variation in a series of electric field spectra obtained during the April 1984 experiment is also plotted. The electric field spectra vary greatly from hour to hour, a consequence of the the strongly varying intensity of the magnetospheric fluctuations. Apparently, some of the time the spectra are dominated by the fields induced by the surface gravity waves; usually, the fields induced by magnetospheric fluctuations are much larger.

Snodgrass et al. [1966] measured long-period surface gravity waves and predicted that the ocean basins should be filled with these waves. These waves are generated by nonlinear processes at the coastlines (usually described as surfbeat) and most of the energy is trapped to the continental shelf as edge waves but some is radiated into the deep sea [*Munk et al.*, 1964]. The waves attenuate very slowly and can travel great distances. Our observations show very similar spectral amplitudes for three different times of year.

The presence of long-period gravity waves will interfere with observations of long-period seismic waves. Even if a seismometer is installed in a deep hole drilled into the seabed, this noise will be severe. The seafloor rocks and sediment will respond to the pressure fluctuations produced by the gravity waves in a similar fashion to the shaking of seismometers on land by atmospheric pressure fluctuations as described by *Sorrels and Goforth* [1973]. The gravity waves can be of large wavelength (20 km at 100 s period), and the perturbations penetrate to great depth. We have plotted in Figure 3 the spectrum of vertical acceleration expected at the seafloor (solid line) and at the bottom of the sediment column at a depth of 770 m below the seafloor (dashed line) that can be forced by typical seafloor pressure fluctuations. We have assumed the

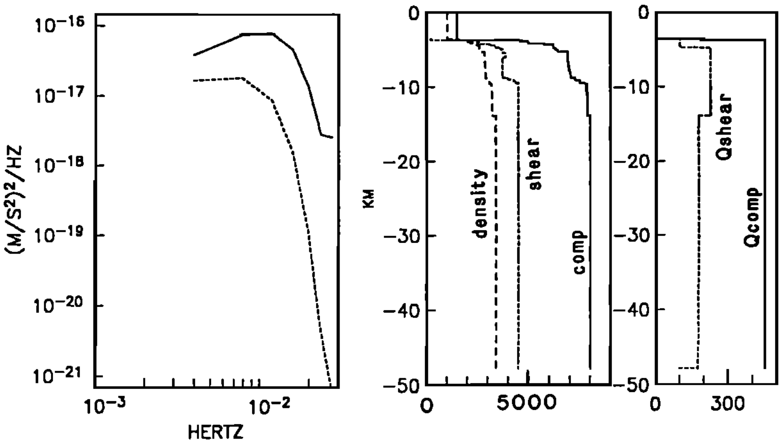

Fig. 3. (Left) A prediction for the power spectrum of ground motion (vertical acceleration) caused by surface gravity waves. Ground motion is predicted at two depths: the seafloor (solid line) and 770 m below the seafloor (dashed line). (Middle) The model used for these calculations. Compressional wave velocity and shear wave velocity in meters per second and density in kilograms per cubic meter are plotted versus depth in kilometers. (Right) A model for Q_α (solid line) and Q_β (dashed line) versus depth in kilometers below the sea surface.

pressure fluctuations are solely caused by surface gravity waves and calculated the response functions for a model of 15-m.y.-old crust [*Spudich and Orcutt*, 1980]. The estimates of vertical acceleration at the two depths begin to diverge at frequencies above 0.015 Hz when the wavelength of the surface gravity waves becomes comparable to the distance below the seafloor.

The pressure disturbance of long-period surface water waves can in principle, on the other hand, provide a source for studies of the response of the earth to known loading. Because the phase velocity of the waves ($\sqrt{gh}$) is small compared to seismic waves of comparable wavelengths, the response will be essentially equivalent to that of static loading. By correlating the pressure and the vertical acceleration (assumed to be measured by a long-period seismograph) as a function of wavelength some elastic properties can in principle to deduced as a function of depth in the earth.

The predicted seafloor acceleration spectrum is comparable to a very noisy land site LJC, which is located right on the coast and slightly noisier than an island station RAR [*Agnew and Berger*, 1978; also *Haubrich*, 1970]. The noise at seafloor stations is 20-30 dB higher than at quiet land sites.

There has been apparently only one marginally successful deployment of a long-period seismograph on the seafloor [*Prothero and Munk*, 1974]. The displacement spectrum observed with this instrument (Figure 32 in the report) shows a rise at periods longer than 40 s, which is consistent with the predicted effect of long-period surface gravity waves.

INTERMEDIATE FREQUENCIES

Both the electric field and pressure spectra show a minimum in spectral energy between 10 and 25 s (see Figure 1). The surface gravity waves are strongly attenuated at the seafloor at these periods as are the magnetospheric fluctuations. The pressure spectrum is 40-45 dB quieter here than at microseism frequencies or at lower frequencies. The depth of the minimum varies greatly from spectrum to spectrum, but much of this variation can be ascribed to "glitches" in the electronic recording system. Careful inspection of records with particularly large spectral levels in this band show sudden jumps in the record but only after the signal has been heavily filtered to remove both the long-period gravity waves and the microseisms. Beyond the simple instrument problem, there are three causes of pressure fluctuations in the frequency band from about 0.03 to 0.1 Hz: (1) long-period acoustic waves in the atmosphere, (2) motions caused by seismic waves generated by the "single frequency" microseism mechanism, and (3) turbulent flow over the transducer and in the bottom boundary layer.

We have plotted an estimate of the spectrum of pressure fluctuations in atmospheric acoustic waves from *Sorrels and Douze* [1974, Figure 4] on Figure 1. These authors used an array of microbarographs to determine the high phase velocity components at a continental site. If these waves exist over the ocean, the pressure fluctuations will penetrate to the seafloor with only slight attenuation because the atmospheric acoustic wave velocity is much greater than $\sqrt{gh}$ (h is the ocean depth). The agreement with our observations suggests that an appreciable part of the noise at intermediate frequencies originates in atmospheric acoustic waves. However, these waves may not be as prevalent over the ocean as over land; *Sorrels and Douze* [1974] cite evidence that these waves principally originate over mountain ranges.

On land there are often peaks observed in microseism spectra which can be directly related to the swell at nearby coasts [*Haubrich et al.*, 1963]. Often two peaks are observed. One is at the same frequency as the swell and is called the "single frequency" peak; the other appears at twice the frequency of the swell. We will discuss the "double frequency" peak extensively later in this paper.

The existence and cause of the single frequency peak was known as early as 1904 and identified with the steepening and breaking of swell at the coast [*Wiechert*, 1904]. This mechanism of forcing seismic surface waves

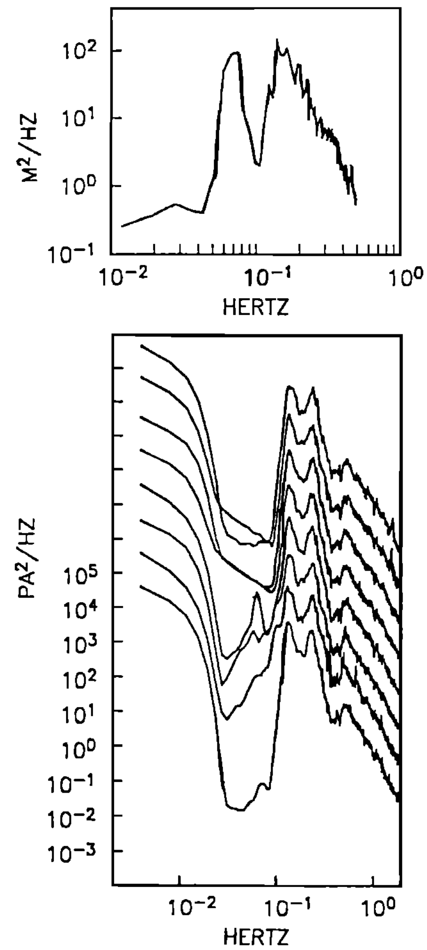

Fig. 4. (Bottom) Eight power spectrum estimates from July 1983. Each spectrum is based on 4096-s of data and is shifted upward one power of ten from the preceding spectrum for clarity. The scale is appropriate for the bottom (first) spectrum in the series. Several spectra exhibit high noise levels of instrumental origin at frequencies between 0.03 and 0.1 Hz. The single frequency microseism peak is apparent at 0.064 Hz in the fourth spectrum. (Top) A

is described by *Hasselmann* [1963]. We observe these seismic waves after they propagate into the deep ocean.

In Figure 4 we present a series of seafloor pressure spectra obtained during the July 1983 experiment. The spectral level in the gap is quite variable, but a substantial peak at 0.064 Hz is observed to develop over a period of a few hours, which then fades back into the background. Some of these spectra are badly contaminated by electronic noise. The wave height spectra from Begg rock show a prominent peak at 0.064 Hz, which persists over the time of the observations. We do not understand why the single frequency peak is observed only briefly and in only this one set of observations.

Turbulent flow in the bottom boundary layer and around the instrument could produce small pressure fluctuations. The spectrum would depend critically on the details of the topography and the flow, but we can estimate the flow necessary to produce the observed pressure fluctuations. For the measured pressure spectrum minimum of 0.03 Pa^2/Hz and a bandwidth of 0.1 Hz the rms pressure fluctuations are $p=$ 0.055 Pa. If they are entirely the result of turbulent eddies in the sea, the rms water speed in the eddies should be of order $\sqrt{p/\rho} = 7$ mm/s, a not unusual flow speed near the seafloor in the eastern Pacific [*Wimbush and Munk*, 1970]. The density of seawater is ρ.

The great variability in the seafloor electric field spectrum at periods longer than 20-30 s can be attributed to the variability of the magnetospheric fluctuations. The deep ocean effectively filters out this cause of electric field fluctuation at shorter periods, and a sharp drop in spectral level is apparent between 0.03 and 0.05 Hz (Figure 2). The quieter spectra from the April experiment show a flat minimum between 10^{-21} and 10^{-20} $(V/m)^2/Hz$ at frequencies between 0.05 and 0.1 Hz. The spectra from the February experiment show slightly higher values in this band (Figure 1). The origin of the energy in this band is a bit mysterious; Rayleigh waves are ineffective generators of electric field fluctuations in this frequency range because Δu (equation (4)) is small (and changes sign). There is also no evidence of Rayleigh wave energy in the pressure spectrum. Love waves, however, will induce a voltage in an antenna lying on the seafloor (see equation (3)). The vertical component of the geomagnetic field in this area is about 4×10^{-5} T, the spectrum of horizontal velocity of the seafloor required to produce the observed field fluctuations is then about 1.6×10^{-21} $(V/m)^2/Hz$ divided by $(4 \times 10^{-5}\ T)^2$ or 10^{-12} $(m/s)^2/Hz$. Ocean bottom seismometer observations of horizontal displacement at frequencies just below the microseism peak are comparable when converted to velocity [*Prothero and Schaecher*, 1984; *Latham and Sutton*, 1966]. The causes of the seafloor motions at these frequencies are not apparent.

MICROSEISMS

The microseism peak is readily apparent in both the electric field and pressure observations. These microseisms are chiefly generated by long-wavelength pressure disturbances at the surface of the ocean created by the nonlinear interaction of surface gravity waves. *Longuet-Higgins* [1950] showed that two trains of waves will produce a traveling disturbance with a wave number equal to the sum of wave numbers $(\mathbf{k}_1+\mathbf{k}_2)$ and a frequency equal to the sum of frequencies $(\omega_1+\omega_2)$. For waves of very similar frequency meeting head on, $\mathbf{k}_1 \approx -\mathbf{k}_2$ so the sum of the wave numbers is small, and the wavelength of the disturbance can be very large. As a consequence of the long horizontal wavelength, the pressure disturbance either reaches the bottom directly or radiates acoustic waves efficiently. In either case the pressure at the seabed is appreciable. The disturbance then has approximately twice the frequency of the surface gravity waves, and the peak in the spectrum generated by this mechanism is described as the "double frequency" peak. The long wavelength of the disturbances generated and the corresponding phase velocity can be sufficiently large for efficient forcing of Rayleigh waves.

Hasselmann [1963] developed a theory for the forcing of Rayleigh waves by the nonlinear interaction of surface gravity waves. *Hughes* [1976)] and *Kadota and Labianca* [1981] have reexamined the problem. *Cox et al.* [1978] focus on the induction of the electric field by microseism motions.

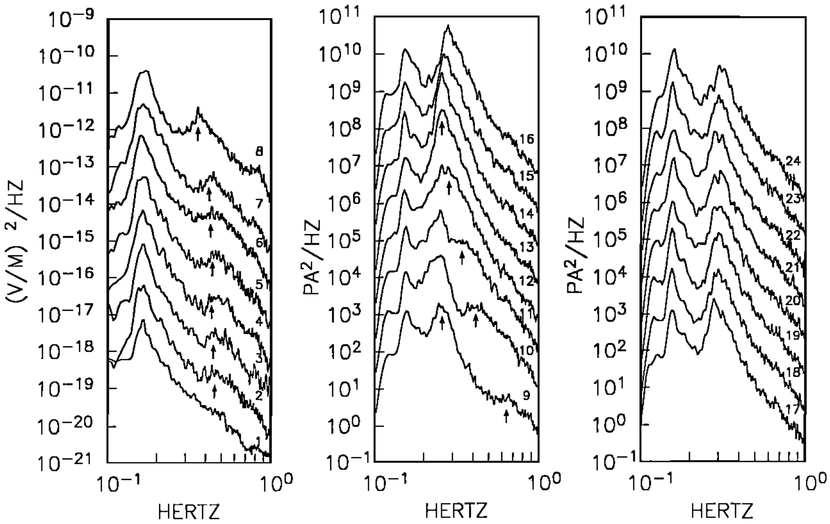

Fig. 5. Eight estimates of the power spectrum of the electric field (left panel) and 16 estimates of the power spectrum of pressure fluctuations (middle and right panels) from the February experiment. The spectra are numbered (Table 2) and are based on data sections 4096-s long. Arrows point to microseism peaks that we relate to the local storm-generated wind wave field. Each panel shows eight spectra plotted one decade apart for clarity. The scales are appropriate for the lowermost spectrum.

Microseisms are generated in regions where surface gravity waves can interact with other waves head on. This can happen near coastlines when swell reflects off the coast. A clear relationship between swell arriving at the coastline and the single and double frequency peaks in the microseism spectrum was demonstrated by *Haubrich et al.* [1963].

Microseisms can also be generated in the open ocean. Observations of the directional spectrum of wind-driven waves show components traveling in almost all directions [*Tyler et al.*, 1974; *Longuet-Higgins et al.*, 1963]. Significant energy appears in waves traveling crosswise to the wind, and these waves in particular are able to interact to produce microseisms.

Microseisms are expected to be generated most effectively under storms where the waves are large and distributed broadly in direction by the varying wind direction in the storm. We have observed the evolution of the seafloor pressure and electric field spectra as a small storm passed above an instrument under 1.5 km of ocean (February 1983). Figure 5 displays a series of spectra of either electric field or pressure fluctuations (both spectra look very similar at all times during the experiment at frequencies between 0.1 and 1 Hz). Each spectrum is based on slightly more than one hour of data (4096 s). The wind was light at the start of this data series but increased to over 15 m/s later in the experiment (see Table 2). We have labeled the spectra in order from 1 to 24. Note that each spectrum is separated from the preceding one by a factor of 10 in the figures for clarity. A small peak is barely discernible at about 0.5 Hz in spectrum 2; in later spectra it is observed to evolve toward lower frequency and much larger amplitude. During the ninth spectrum the wind shifted direction about 120°. A second peak appears at about 0.5 Hz, which also is seen to shift toward lower frequency and much larger amplitude in later times. It eventually merges with the first peak.

The peaks from selected electric field spectra have been sketched in Figure 6 to demonstrate more clearly the development of the two peaks. The small bump seen in spectrum 3 becomes a much larger peak by the time of spectrum 10, and the frequency of the peak is much lower. The second peak that begins developing after the wind shifts during spectrum 9 also appears in spectrum 10. This spectral peak develops in a similar fashion to the first

TABLE 2 February Spectra

No	Date	Start Time	Wind, m/s		Notes
1	Feb 1	1438	5	130°	
2	Feb. 1	1555	5	130°	
3	Feb. 1	1724	6	130°	
4	Feb. 1	1828	6.5	130°	
5	Feb 1	1945	7	130°	
6	Feb. 1	2054	7.5	130°	
7	Feb. 1	2153	7.5	120°	
8	Feb. 2	0612	9-15	125°	gap in data, wind gusts to 50 knots
9	Feb. 2	0808	15	125°	
10	Feb. 2	0921	10	240°	large shift in the wind direction
11	Feb. 3	1029	10	240°	
12	Feb. 3	1138	10	240°	
13	Feb. 3	1246	11.5	240°	
13	Feb. 3	1358	12.5	240°	
15	Feb. 3	1507	12.5	240°	
16	Feb. 3	1615	12.5	240°	
17	Feb. 3	1715	12.5	240°	
18	Feb. 3	1823	12 5	240°	
19	Feb. 3	1934	12.5	240°	
20	Feb 3	2044	7.5	240°	
21	Feb. 3	2152	7 5	240°	
22	Feb. 3	0014	5	220°	
23	Feb. 3	0122	2 5	220°	
24	Feb. 3	0231	calm		

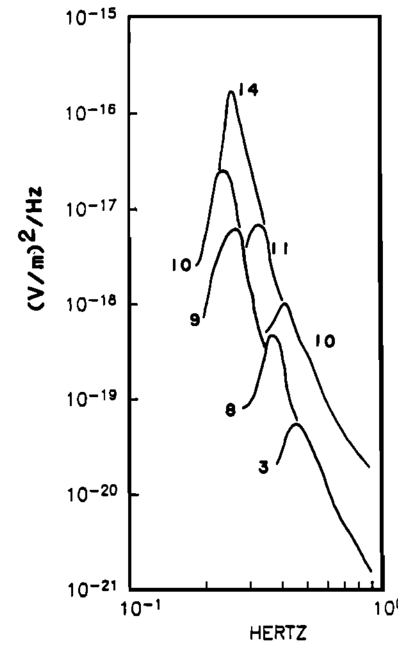

Fig. 6. A sketch of selected electric field spectra from the February experiment showing the two storm-related microseism peaks.

peak, reaching a maximum in spectrum 14. The envelope of both sets of curves follows a f^{-7} power law in frequency, but the second peak is larger by about a factor of 8. This difference can be well explained by the much larger interaction possible in the confused sea left by the change in wind direction.

A very recent paper by *Kibblewhite and Ewans* [1985] describes observations from a long-period seismograph installed in shallow water (100 m) which show the microseism spectra evolving during storms.

Hasselmann [1963] derives an equation for the wave number and frequency spectrum $\mathbf{P}_s(\mathbf{k},\omega)$ of the pressure fluctuations on a level surface just below the sea surface driven by a surface gravity wave field with the wave height spectrum $\mathbf{Z}(\omega,\theta)$:

$$\mathbf{P}_s(\mathbf{k},\omega)=\frac{\rho^2g^2\omega}{2}\int_{-\pi}^{\pi}\mathbf{Z}(\omega/2,\theta)\mathbf{Z}(\omega/2,\theta+\pi)d\theta \qquad (6)$$

The pressure fluctuations are driven at twice the frequency of the waves in the height spectrum. Waves traveling in the direction θ interact with waves traveling in the direction $\theta+\pi$. The surface pressure spectrum is white in wave number; the wave number does not appear explicitly in equation (6). This is an approximation valid for the small wave number waves which can be felt at the deep seafloor.

In general, this surface forcing will drive Rayleigh wave modes resonantly, and only these modes will propagate to large distances from the source region. We choose to separate locally forced microseisms where the motions caused by the surface forcing dominate over the effects of the free waves from the more typical case where the dominant signal represents some sum over free waves driven by resonant forcing over a broad area. We return to the problem of resonantly driven modes later.

For now we choose to ignore the resonant interactions. This is probably a good approximation in describing the microseisms generated by the small storm in February 1983 for several reasons: (1) the observations were made in an area of rough topography which should scatter the modes intensely, and (2) the storm was of fairly small size and the free waves should quickly travel out of the forcing region, limiting their amplitude.

Within the ocean the forced waves are governed by a wave equation:

$$\nabla^2 p=\frac{1}{\alpha^2}\frac{\partial^2 p}{\partial^2 t} \qquad (7)$$

where α is the speed of sound in seawater. A traveling wave solution for this equation is

$$p=Ae^{i(\mathbf{k}\cdot\mathbf{x}-\omega t+rz)} \qquad (8)$$

$$r=(\frac{\omega^2}{\alpha^2}-|\mathbf{k}|^2)^{1/2}$$

For $|\mathbf{k}|<\omega/\alpha$ the solution is trigonometric in z and the amplitude is independent of depth. For $|\mathbf{k}|>\omega/\alpha$ a solution forced at the surface will attenuate exponentially with depth. For a very deep ocean we expect only waves with wave numbers less than ω/α to reach the seafloor. With this reasoning we can estimate the frequency spectrum of pressure in the deep ocean by integrating the surface frequency-wave number spectrum (equation (6)) over all $|\mathbf{k}|<\omega/\alpha$:

$$P_d(\omega)=\frac{\pi\rho^2g^2\omega^3}{2\alpha^2}\int_{-\pi}^{\pi}\mathbf{Z}(\omega/2,\theta)\mathbf{Z}(\omega/2,\theta+\pi)d\theta \qquad (9)$$

We follow *Tyler et al.* [1974] in deriving this expression. We have ignored the effects of finite ocean depth. This expression is the same as equation (1) of *Kibblewhite and Ewans* [1985].

Ideally, we should directly compare the microseism spectra with observations of the wind wave spectrum, but the Begg Rock buoy is too far away to provide a useful measure of the local wind wave field. Observations of the wave height spectrum of wind-driven surface gravity waves show that for a steady wind the spectrum quickly approaches an equilibrium spectrum which depends only on the fetch and wind velocity. Many descriptions of the evolution of wind-driven waves have been published; we will use the description of *Hasselmann et al.* [1973] of the JONSWAP observations.

$$\mathbf{W}(f)=ag^2(2\pi)^{-4}f^{-5}\exp[\frac{-5}{4}(\frac{f}{f_m})^{-4}]\,\gamma^d$$

$$d=\exp\left[\frac{-(f-f_m)^2}{2\sigma^2f_m^2}\right] \qquad \sigma=\begin{cases}\sigma_a & f\leqslant f_m\\ \sigma_b & f>f_m\end{cases} \qquad (10)$$

The wave height spectrum increases with decreasing frequency following f^{-5} power law. The spectrum cuts off sharply at frequencies just below some sharply defined frequency f_m. This formulation begins with five free parameters f_m, a, γ, σ_a, σ_b, but we follow *Hasselmann et al.* and fix $\gamma=3.3$, $\sigma_a=0.07$, and $\sigma_b=0.09$. Note that f and f_m are frequencies in hertz in equation (10). This spectrum differs from the *Pierson and Moskowitz* [1964] spectrum by a factor which enhances the spectral level near

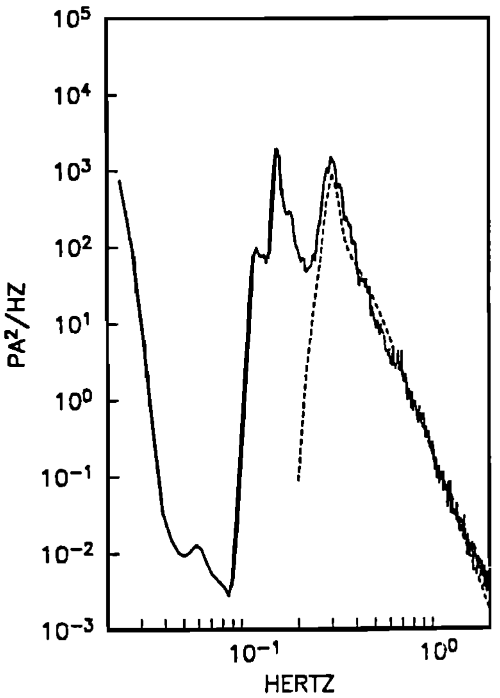

Fig. 7. Pressure spectrum 19 (see Table 2) is plotted (solid line) with a prediction (dashed line) from equation (14) with the beam parameter (q) set to two.

the peak in the spectrum at frequency f_m. This factor represents an increase of a factor of 3.3 in the peak value of the wave height spectrum and more than a factor of 10 in the prediction for the microseism spectrum which depends on the square of the wave height spectrum (equation (6)). The spectrum is a function of two parameters, a which determines the amplitude of the spectrum and f_m. These parameters have been empirically related by a power law which is also a function of U_{10}, the wind velocity at 10 m height. We have frequent ship observations of the wind velocity during the storm. We fit the microseism spectrum to determine f_m and then determine a from the power law. In this way the unknown effects of fetch and duration are subsumed under the observable f_m.

The microseism spectrum also depends on the directional dependence of the wind wave field. *Longuet-Higgins et al.* [1963] suggest a form for the directional dependence of the spectrum:

$$\mathbf{G} = \cos^q[(\theta-\theta_0)/2]/H \qquad -\pi \leqslant \theta < \pi \qquad q = q(f) \tag{11}$$

with the normalization factor H such that

$$\int_{-\pi}^{\pi} \mathbf{G}(\theta)d\theta = 1 \qquad H = 2\pi^{1/2}\frac{\Gamma(\frac{q+1}{2})}{\Gamma(\frac{q}{2}+1)} \tag{12}$$

The frequency directional spectrum is then

$$\mathbf{Z}(f,\theta) = \mathbf{W}(f)\mathbf{G}(\theta) \tag{13}$$

After changing in equation (9) from frequency in radians per second to hertz, we find for the seafloor pressure spectrum,

$$\mathbf{P}_b(f) = \frac{2g^2\pi^3\rho^2 f^3}{\alpha^2}\mathbf{W}^2(f/2)\mathbf{I}[q(f/2)] \tag{14}$$

where

$$\mathbf{I}(q) = \int_{-\pi}^{\pi} \mathbf{G}(\theta)\mathbf{G}(\theta+\pi)d\theta = 2^{-1-q}\pi^{-1/2}\frac{\Gamma(\frac{q}{2}+1)}{\Gamma(\frac{q+1}{2})} \tag{15}$$

At frequencies away from the spectral peak, $q=2$ is an adequate fit to wave observations. In Figure 7 we have plotted a microseism spectrum predicted from equation (14), with $q=2$ and f_m determined by the peak measured from spectrum 19 (see Table 2). We also plot spectrum 19 (solid line). The two spectra are very similar; the fit is excellent over five decades in the spectral density and over a decade in frequency. The f^{-7} power law at higher frequencies is apparent along with the enhancement near the peak.

Equation (14) can be inverted and q determined from the observations:

$$\mathbf{I}[q(f/2)] = \mathbf{P}_b(f)\frac{\alpha^2}{2\rho^2 g^2\pi^3 f^3\mathbf{W}^2(f/2)} = \mathbf{L}(f) \tag{16}$$

$$q(f/2) = \mathbf{I}^{-1}[\mathbf{L}(f)]$$

In Figure 8 we plot q versus frequency for three of the spectra in Table 2 (spectra 9, 14, and 19). Spectra 9 was obtained near the beginning of the experiment. The wind had been from the same direction, but steadily increasing for half a day. The beam parameter is small at high frequencies, increasing to about five near the peak in the spectrum in rough agreement with typical values for the beam parameter derived from direct measurements of surface gravity wave height spectra [*Tyler et al.*, 1974]. At some frequencies the microseism spectrum is too large to fit to equation (16) (then q is set to zero), suggesting that either equation (11) is not an adequate expression for the wind directional spectrum or more likely that this is just

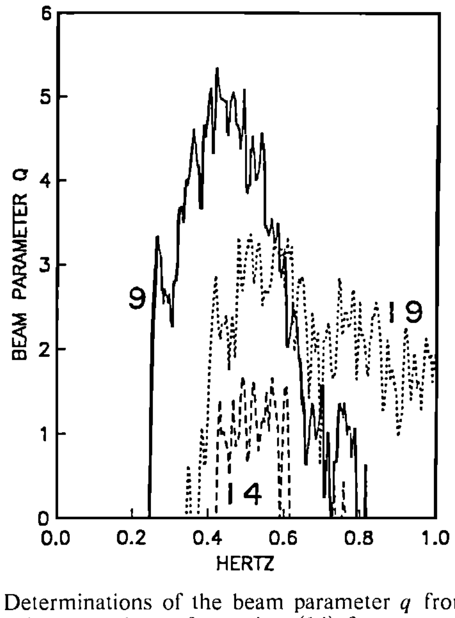

Fig 8. Determinations of the beam parameter q from observations and the predictions of equation (14) for spectra 9, 14, and 19.

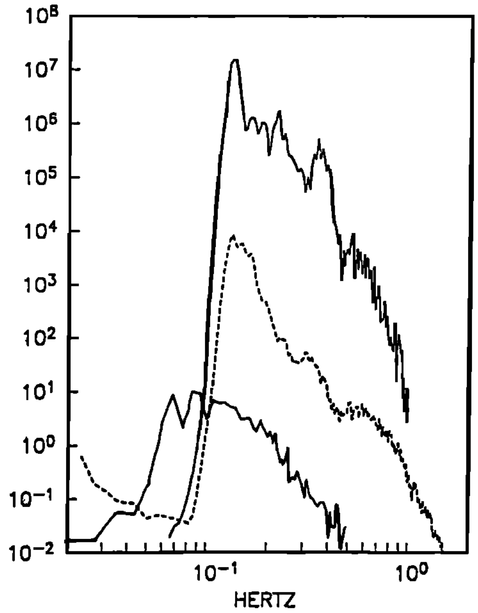

Fig. 9. One realization of the power spectrum of pressure fluctuations in Pa^2/Hz (dashed line), and wave height in m^2/Hz (lower solid line) from April 1984. Also plotted a "prediction" for the seafloor pressure spectrum (upper solid line). The prediction is an arbitrarily scaled calculation in which the pressure transfer function is multiplied by the square of the wave height spectrum observed at Begg Rock evaluated at half the frequency.

too simple an analysis to account for the forcing of microseisms in a real finite depth ocean. It is still interesting to see the much smaller values for q predicted after the wind abruptly shifts direction and a new wave spectral peak develops (spectrum 14). Much later in the experiment the predicted q increases back toward the original values predicted by spectrum 9 (spectrum 19). The wind is steady for many hours before spectrum 19, presumably, the old wind waves generated before the change in wind direction have propagated out of the region and so the nonlinear interaction that creates the microseisms is reduced back toward the original intensity.

SURFACE WAVE MODES AND MICROSEISMS

The seafloor pressure fluctuations observed during the February experiment can be completely explained by the surface forcing. The local forcing drives seismic waves of all wave numbers, but only very particular wave numbers correspond to freely propagating waves. Evidence for these resonant modes is not apparent in the seafloor pressure fluctuations observed during the February 1983 experiment. In contrast, in the July 1983 and April 1984 experiments, ground motion caused by seismic surface waves propagating in from other regions appears to be the dominant cause of pressure and electric field fluctuations. In this section we will describe the two deep-water experiments and a theory for the forcing of surface wave modes by a distributed surface pressure field.

Haubrich et al. [1963] and many other authors have found a clear relationship between peaks in the microseism spectrum and swell at half the frequency. This relationship is also very evident in some of the seafloor observations. But there are also several peaks in the microseism spectrum which appear to be totally unrelated to the shape of the swell spectrum. These peaks we will show are caused by modes of seismic surface waves with energy trapped near the seafloor, in the very upper layers of sediment.

Spectra of pressure (Figure 9) and electric field (Figure 1) fluctuations from data collected at the beginning of the April cruise show a peak near 0.14 Hz which is also seen in the wave height spectrum at 0.07 Hz (Figure 9). This peak was observed to drift slowly toward higher frequency over a period of three days (see *Webb and Cox* [1984] for details). This microseism peak is caused by the interaction of the swell with swell reflected back off the coast. We can identify the source of the swell as a storm in the northeast Pacific. The waves are dispersed, and the distance (6300 km) to the storm can be determined by the rate of shift of the frequency of the microseism peak (see *Snodgrass et al.* [1966] for a discussion of the dispersion of swell).

There are bumps on the pressure spectrum at 0.3 and 0.5 Hz and on the electric field spectrum at 0.4 and 1 Hz which do not seem to be related to peaks in the swell spectrum. Begg Rock is sufficiently far from the experiment sites that dissimilarity between the swell and the microseism spectra is not unexpected. However, the peaks in the electric field spectrum and the pressure spectrum do not coincide, which suggests a different origin.

Pressure spectra from the July 1983 experiment again show a peak at 0.4 Hz, which is apparently not related to the shape of the local swell spectrum (Figure 4). To explain these peaks, we examine the properties of seismic surface wave modes in an oceanic earth model.

A Green's function describing the excitation of Rayleigh wave modes by point sources in a layered earth model can be easily calculated using the theory of *Takeuchi and Saito* [1972] (see also *Aki and Richards* [1980]). The displacements, stresses, and pressure in the ocean at a receiver at the origin of the x, y plane and at a depth z_0 caused by a point force at location $\mathbf{r}$, can be described by Green's functions:

$$u_i(\omega)=f_l \mathbf{G}_{il}(\mathbf{r};z_0,\omega) \qquad (17)$$
$$P(\omega)=f_l \mathbf{G}^P_l(\mathbf{r};z_0,\omega)$$

where $u_i(\omega)$ is the Fourier transform in frequency of the ith component of displacement and $f_l(\omega)$ is the Fourier transform of the lth component of the point force.

The electric field caused by the motion of the seafloor and ocean through the geomagnetic field ($\mathbf{F}$), is linearly related to the displacements, and a Green's function can be defined. To a good approximation the field measured by an antenna lying on the seafloor is

$$\mathbf{E} \approx (\mathbf{v}_s - \mathbf{v}_w) \times \mathbf{F} \qquad (18)$$

where $\mathbf{v}_s$ is the seafloor particle velocity and $\mathbf{v}_w$ is the velocity in the seawater just above the seafloor. On the horizontal seafloor the difference $(\mathbf{v}_s - \mathbf{v}_w)$ is strictly horizontal because the vertical velocity is continuous at the interface. The electric field Green's functions can be defined in terms of the displacement Green's functions. Let z_{0+} be a depth just above the seafloor, z_{0-} a depth just below the interface, and ϵ_{ijk} be the permutation operator:

$$\mathbf{E}_k(\omega)=\epsilon_{ijk}\mathbf{F}_j f_l(\omega)\Big[i\omega\mathbf{G}_{il}(\mathbf{r};z_{0+},\omega)-i\omega\mathbf{G}_{il}(\mathbf{r};z_{0-},\omega)\Big]$$

$$=\mathbf{F}_j f_l(\omega)\mathbf{G}^E_{ljk}(\mathbf{r};z_0,\omega) \quad (19)$$

A distributed pressure field at the sea surface can be expressed as as integral over vertical point forces; we now drop the l index. For a vertical point force source any of these Green's functions can be written as a sum over Rayleigh wave modes. The problem fits naturally into cylindrical coordinates $\mathbf{r}=(r,\phi,z)$:

$$p(\omega)=f(\omega)\sum_n \mathbf{G}^p_n(z;z_0,\omega)\mathrm{J}_0(k_n r) \quad (20)$$

where J_0 is the Bessel function of zero order and k_n is the wave number of the nth Rayleigh mode. The two orthogonal components of the electric field at the origin are

$$\mathbf{E}_1=\mathbf{F}_3 f(\omega)\sum_n \mathbf{G}^E_n(z;z_0,\omega)\mathrm{J}_0(k_n r)\cos(\phi)$$

$$\mathbf{E}_2=\mathbf{F}_3 f(\omega)\sum_n \mathbf{G}^E_n(z;z_0,\omega)\mathrm{J}_0(k_n r)\sin(\phi) \quad (21)$$

The pressure fluctuations at the receiver caused by a pressure field $\mathbf{P}(r,\phi,\omega)$ distributed over an area of the free surface is written as an integral over the area Γ:

$$p(\omega)=\int\Gamma\sum_n \mathbf{G}^p_n(0;z_0,\omega)\mathrm{J}_0(k_n r)\mathbf{P}(r,\phi,\omega)\,r\,dr\,d\phi \quad (22)$$

and there is a similar expression for the electric field and the displacements.

An average over an ensemble of possible pressure fields will result in an estimate for the frequency spectrum of the pressure at the receiver:

$$\mathbf{P}_b(\omega)=\langle p^*(\omega)p(\omega)\rangle \quad (23)$$

$$\mathbf{P}_b(\omega)=\int\Gamma\int\Gamma\sum_n\sum_m \mathbf{G}^p_n\mathbf{G}^{p*}_m\mathrm{J}_0(k_n r)\mathrm{J}_0(k_m r') \quad (24)$$

$$\cdot\langle\mathbf{P}(r,\phi,\omega)\mathbf{P}^*(r',\phi',\omega)\rangle\, r\,dr\,r'\,dr'\,d\phi\,d\phi'$$

The quantity

$$\langle\mathbf{P}(r,\phi,\omega)\mathbf{P}^*(r',\phi',\omega)\rangle \quad (25)$$

is recognized as the autocorrelation of $\mathbf{P}$. *Hasselmann*'s [1963] expression for the frequency wave number spectrum of the surface forcing (equation (6)) suggests that the spectrum is nearly white in wave number. A not unreasonable estimate for the autocorrelation of $\mathbf{P}$ is then

$$\langle\mathbf{P}^*(\mathbf{r})\mathbf{P}(\mathbf{r}')\rangle=\mathbf{C}(\omega)\delta(\mathbf{r}-\mathbf{r}') \quad (26)$$

where

$$\mathbf{C}(\omega)=\frac{(2\pi)^2\rho^2 g^2\omega}{2}\int_{-\pi}^{\pi}\mathbf{Z}(\omega/2,\theta)\mathbf{Z}(\omega/2,\theta+\pi)\,d\theta \quad (27)$$

where again $\mathbf{Z}(\omega,\theta)$ is the frequency and direction spectrum of the surface wave field. We require that the pressure field created by the nonlinear interactions of surface waves be uncorrelated at the sea surface over distances comparable to the wavelength of Rayleigh waves. Probably, we should allow $\mathbf{C}(\omega)$ to be a slowly varying function of position to allow for changes in the wave field. The pressure field at the seafloor created by the Rayleigh waves may be correlated over reasonable distances, since the Green's functions select particular wave numbers.

The double integral in equation (24) simplifies to a single integral. For some simple region geometries, the terms in the double sum over n and m can be shown to be small if $m\neq n$ and if the generating region is reasonably large. For a very simple model which places the receiver at the center of a uniform forcing region with boundaries defined by $R(\phi)$, equation (24) reduces to

$$\mathbf{P}_b(\omega)=C(\omega)\sum_n\frac{|\mathbf{G}^p_n(z_0;0,\omega)|^2}{\pi k_n}\int_0^{2\pi}R(\phi)\,d\phi \quad (28)$$

The spectrum of a horizontal component of the electric field is similarly

$$\mathbf{E}_b(\omega)=C(\omega)\sum_n\frac{|\mathbf{G}^E_n(z_0;0,\omega)|^2}{\pi k_n}\int_0^{2\pi}R(\phi)\cos^2(\phi)\,d\phi \quad (29)$$

Written out more completely, the bottom pressure spectrum is related to the surface wave height spectrum by

$$\mathbf{P}_b(\omega)=2\pi^2\rho^2 g^2\omega\int_{-\pi}^{\pi}\mathbf{Z}(\omega/2,\theta)\mathbf{Z}(\omega/2,\theta+\pi)\,d\theta \quad (30)$$

$$\cdot\sum_n\frac{|\mathbf{G}^p_n(z_0;0,\omega)|^2}{\pi k_n}\int_0^{2\pi}R(\phi)\,d\phi$$

A model for seismic waves from a distant storm would take a region bounded by radii r_1 and r_2 and azimuths θ_1 and θ_2 with $\Delta\theta=\theta_1-\theta_2$ small. The seismic waves from the region are then nearly planar. The pressure spectrum is then

$$\mathbf{P}_b(\omega)=C(\omega)\sum_n\frac{|\mathbf{G}^p_n(z_0;0,\omega)|^2}{\pi k_n}R\Delta\theta \quad (31)$$

with $R=r_1-r_2$. The linear relationship on R agrees with the results of *Hasselmann*'s [1963] description of linear growth with distance along a ray of the energy in a wave packet.

Returning to equation (30), we note that in general we have measurements of the frequency spectrum $\mathbf{W}(\omega)$ of wave height but not the directional spectrum $\mathbf{G}(\theta)$:

$$\mathbf{Z}(\omega,\theta)=W(\omega)\mathbf{G}(\theta,\omega) \quad (32)$$

$$\int_{-\pi}^{\pi}\mathbf{Z}(\omega/2,\theta)\mathbf{Z}(\omega/2,\theta+\pi)\,d\theta=W^2(\omega/2)N(\omega)$$

where $N(\omega)$ is unknown.

In general we will know little about the size of the generating region but take

$$\int_0^{2\pi}R(\phi)\,d\phi=R_0 \quad (33)$$

and

$$\int_0^{2\pi}R(\phi)\cos^2(\phi)\,d\phi=R^E_0$$

The bottom pressure spectrum is then

$$\mathbf{P}_b(\omega)=\left[2\pi^2 g^2\omega W^2(\omega/2)\sum_n\frac{|\mathbf{G}^p_n|^2}{\pi k_n}\right]N(\omega)R_0 \quad (34)$$

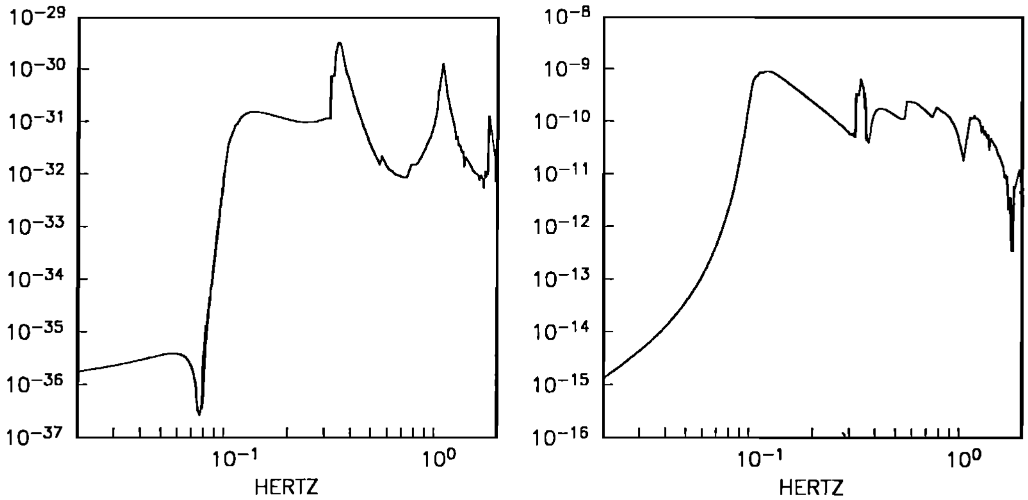

Fig. 10. The electric field (left) and pressure (right) transfer functions versus frequency.

The quantity in the brackets we can evaluate, the rest we hope is a slowly varying function of frequency so that peaks in the observed spectra can be related to the Green's functions and not to the details of the directionality of the wave field ($N(\omega)$) or the distribution of forcing over the ocean (R_0).

The coherence between the electric field and the pressure fluctuations has been measured and is less than 0.2 in the microseism peak. The low coherence suggests that the seismic wave field is not narrowly distributed in direction of propagation. An isotropic wave field would suggest a constant for $R(\phi)$, and then $R_0^E = R_0/2$ (see equation (33)). The ratio of the spectrum of the electric field to the spectrum of pressure is then just a function of the Green's functions:

$$\frac{\mathbf{E}_b(\omega)}{\mathbf{P}_b(\omega)} = \frac{\frac{1}{2}\sum_n \frac{|\mathbf{G}_n^E|^2}{\pi k_n}}{\sum_n \frac{|\mathbf{G}_n^p|^2}{\pi k_n}} = \frac{T^E(\omega)}{T^p(\omega)} \qquad (35)$$

We plot T^E and T^p (which we will call transfer functions) in Figure 10. They are calculated for a layered earth model based on the oceanic model in Figure 3. The transfer functions are derived indirectly from a computer program written by G. Masters. We have not included the effects of gravity, which are not expected to be important. The sound channel in the ocean has been ignored; its effect is small at frequencies below a few hertz.

At low frequency the transfer functions are dominated by the fundamental mode, and the transfer function for pressure falls off sharply with decreasing frequency. The roll off occurs because the vertical wavelength in the ocean becomes large compared to the ocean depth.

The February data were collected in water 1.5 km deep, and the pressure transfer function rolls off sharply at frequencies below 0.2 Hz. This roll off is not apparent in the pressure spectra measured in February (Figure 1) which may be further evidence that the direct effect of the surface forcing is being observed in this experiment. The very rough local topography may make this conclusion from the layered model inapplicable.

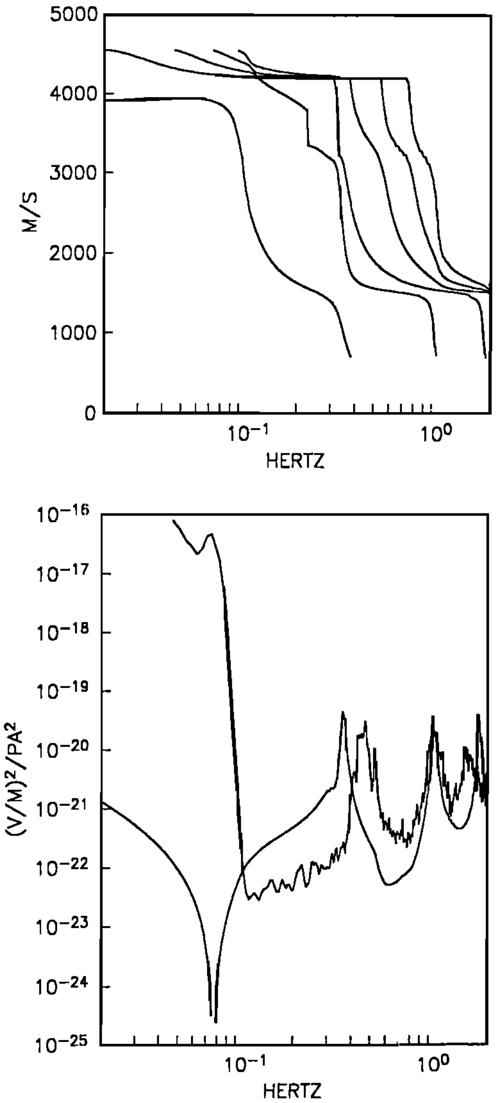

Fig. 11. (Top) Phase velocity for the first several Rayleigh wave modes is plotted versus frequency. (Bottom) The ratio of the electric field transfer function to the pressure transfer function is plotted as a function of frequency. Also plotted is one realization of the ratio of the electric field spectrum divided by the pressure spectrum from data obtained April 1984.

TABLE 3. Base Model for Surface Wave Calculations

Layer Thickness, km	Density, kg/m^3	Compressional Wave Velocity, km/s	Shear Wave Velocity, km/s
3.6	1040.	1.52	0.
0.17	1500.	1.58	0.25
0.23	1990.	4.6	2.2
0.03	2150.	5.	2.2
0.17	2150.	5.	2.65
0.19	2430.	5.75	3.1
0.35	2600.	6.2	3.35
4 1	2800.	6.5	3.75
1.98	3150.	7.7	4.4
3.	3220.	7.84	4.5
34.	3400.	8.	4.5
175.	3400.	7.6	4.2
	3500.	8.2	4.55

Large peaks in the electric field transfer functions at 0.4 and 1 Hz are in rough correspondence to peaks in the electric field spectrum from April (Figure 1). The peak at 0.25 Hz and the troughs at 1 and 1.8 Hz in the pressure transfer function also seem to fit peaks and troughs in the seafloor pressure spectrum (Figure 9). Similarly, the peak at 0.25 Hz in the July 1983 pressure spectrum corresponds to the peak in the transfer function (Figure 4).

We can calculate the ratio of the electric field spectrum to the pressure spectrum (Figure 11). The three peaks in the ratio appear both in the prediction and the observation. Below 0.1 Hz the two spectra are probably determined by different processes. A plot of the phase velocities of the first several Rayleigh wave modes provides an explanation for the peaks (Figure 11). The peaks occur when the phase velocity of the fundamental, first, or second mode becomes smaller than the speed of sound in the ocean. The energy becomes progressively more tightly trapped to the seafloor with increasing frequency and the seafloor motion becomes more and more horizontal. The ratio of horizontal particle motion to pressure becomes large. The electric field is directly related to the horizontal particle velocity. On the high-frequency side of each peak the mode has become too tightly trapped to the seafloor to be forced efficiently by a source at the sea surface, and other modes dominate the transfer functions.

Below 0.3 Hz the transfer functions are dominated by the fundamental or zero mode. Since most of the energy in the seafloor spectra is at frequencies between 0.1 and 0.3 Hz this agrees well with the observations of *Latham and Sutton* [1966] and *Latham and Nowroozi* [1968], who found that the seafloor particle motion was appropriate for waves of the fundamental mode.

Between 0.3 and 1 Hz the first overtone mode has the most energy. At about 0.9 Hz, a wave of this mode causes no fluctuation in the pressure at the seafloor, and a trough appears in the transfer function. This trough does not seem to be well developed in the observations, but deviations from a plane, layered earth should blur over the trough.

The various peaks and troughs in the transfer functions are very sensitive to the shear velocity and thicknesses of the very upper layers of sediment in the model. The ratio of electric field to pressure should be relatively insensitive to the details of the wind wave field (see equation (35)) and is a convenient parameter to use when searching for the best fitting earth model.

We have examined results from a large series of models based on a simplified version of the model in Figure 3 (the base model is defined in Table 3). The locations of the peaks of the electric field to pressure spectral ratio in frequency are totally insensitive to small changes in the water depth. The parameters which determine the frequencies of the peaks are the thickness and shear velocity of the very uppermost layer of sediment and the shear velocity in the second layer. To get peaks at all, a thin layer of very slow shear velocity sediment is required.

In Figure 12 we plot the electric field to pressure spectral ratio for several models which differ only by the shear velocity in the shallowest layer of sediment. A slower shear velocity in the top layer shifts the peaks toward lower frequency. We have also examined three models with the same shear velocity but different layer thicknesses. The peaks appear at lower frequency in models with a thicker top layer of sediment. These two sets of information are condensed on a single figure (Figure 13) which shows the frequencies of the first two peaks in the spectral ratio as a function of the thickness and shear velocity in the top layer of sediment.

Peaks appear in the observations of the electric field to pressure spectral ratio from the April experiment at 0.43, 1.05, and 1.7 Hz. To fit the two lower frequency peaks, we take the thickness of the first sediment layer to be 100 m and the shear velocity to be 200 m/s. The third peak is still poorly fit by this model.

The only other parameter which strongly effects the frequencies of the peaks in the spectral ratio is the shear velocity in the second layer (see Figure 13*b*). The lowest frequency peak is virtually uneffected by changes in the

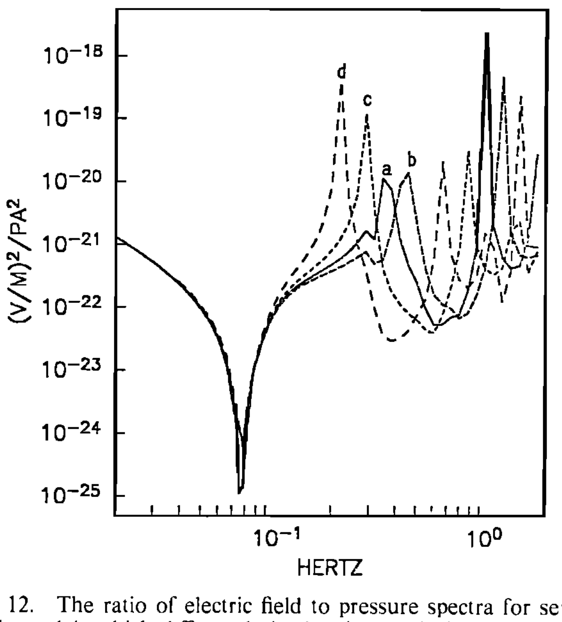

Fig. 12. The ratio of electric field to pressure spectra for several earth models which differ only in the shear velocity in the uppermost layer of sediment. The base model from table 3 (curve a) is compared with other models: 0.30 km/s (curve b); 0.20 km/s (curve c); and 0.15 km/s (curve d).

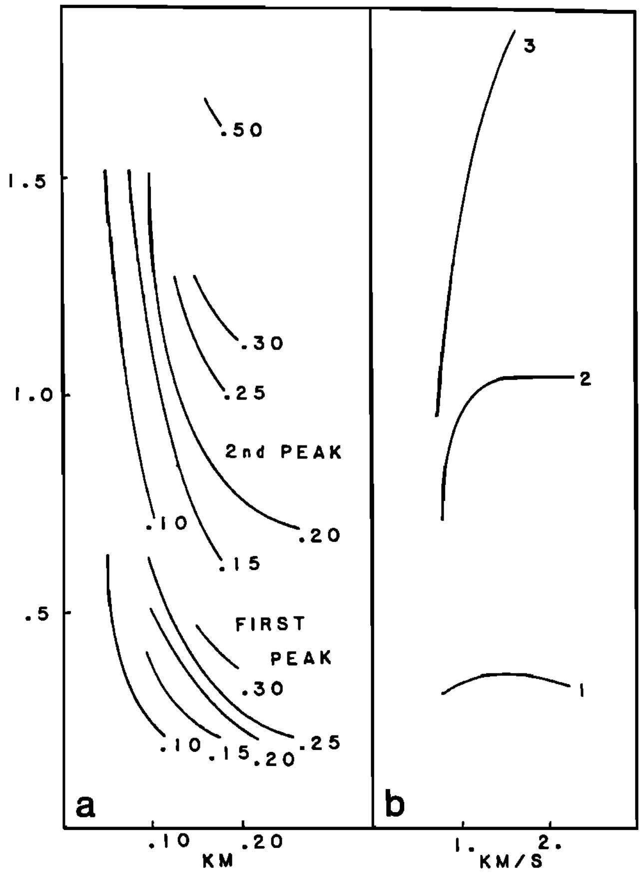

Fig. 13. (*a*) The relationship of the frequencies of the peaks in the ratio of electric field to pressure spectra ratio to the thickness and shear velocity of the uppermost layer of sediment. Frequency of the peaks is plotted versus the layer thickness, and lines of constant shear velocity (in kilometers per second) are labeled. (*b*) Frequency of the first three peaks in the ratio of electric field to pressure spectra versus shear velocity in the second layer of sediment.

shear velocity in this layer but the highest frequency peak can be shifted over a large range of frequencies.

Our final model takes the shear velocity in the second layer of sediments to be 850 m/s. The fit to the April data is quite good (Figure 14). The model does not fit the third peak very well, but the electric field spectra are dominated by instrumental noise above 2 Hz, and we also expect the effects of an unrealistic earth model (flat homogeneous layers) to be more of a problem at higher frequencies. The electric field to pressure spectral ratio is poorly predicted between 0.1 and 0.3 Hz. No reasonable changes in the model will change the predicted ratio. The assumption of isotropy for the seismic wave field may be incorrect. This assumption leads to a factor of one half in equation (35), but for anisotropic wave field this factor can range from zero to one and so there need not be anything wrong with our choice of earth models.

This modeling effort suggests that there must be a fairly thin (100 m) layer of very slow shear velocity (200 m/s) sediment beneath the April site and also that the shear velocity is still fairly slow (850 m/s) at depths greater than 100 m. *Bradner* [1963] suggested that sediment structure could be determined by observing the ratio of horizontal to vertical displacement in microseisms, a measurement very similar to the ratio of electric field to pressure.

We combine the calculated transfer function with the wave spectra observed at Begg Rock in Figure 9. The pressure spectrum has been calculated from equation (34) with an arbitrary multiplicative constant to represent the product NR_0. The several peaks and troughs in the observed spectrum are well modeled by the prediction because we choose the model which fit best. The very sharp drop in spectral level below 0.1 Hz occurs because there is essentially no energy in surface gravity waves at periods longer than 20 s. The roll off in the transfer function at 0.1 Hz also reduces the predicted spectrum at the lowest frequencies. The slope of the predicted spectrum is steeper than the slope observed in the spectrum from the April data. This agrees well with our preconceptions that the lower-frequency surface gravity waves should be more directional and so less efficient at generating microseisms than higher-frequency waves (thus $N(\omega)$ increases with frequency).

Seismic surface waves attenuate very slowly with distance. The spatial Q for Rayleigh waves can be calculated from a vertical integral over the Q for shear waves (Q_β), and compressional waves (Q_α [*Aki and Richards*, 1980, equation 7.89]). The attenuation coefficient (one over the e-folding distance) is related to the spatial Q of a mode by

$$\gamma_n = \frac{\omega}{2CQ_n} \tag{36}$$

with C the phase velocity. A model for Q_α and Q_β is plotted in Figure 3. Attenuation in the ocean is very small; Q_α has been set to infinity, Q_β is undefined. The attenuation coefficients for the first several modes are plotted in Fig-

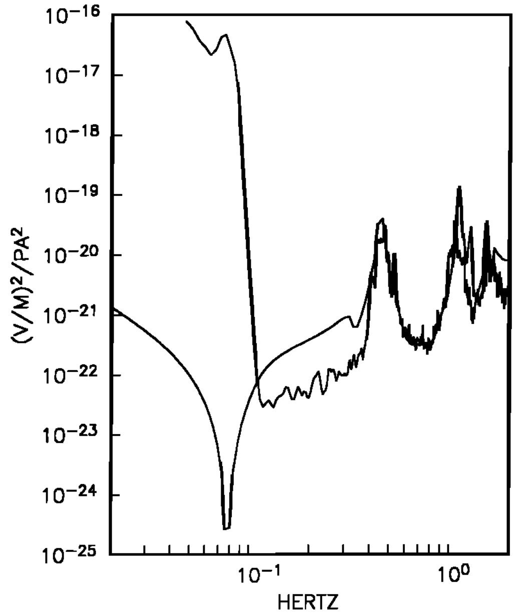

Fig. 14. Best fitting model of the ratio of electric field to pressure spectral ratio is plotted along with one measurement. Model parameters differ from Table 3 in the uppermost sediment layer (thickness = 100 m, shear velocity = 200 m/s) and in the second layer (shear velocity = 850 m/s).

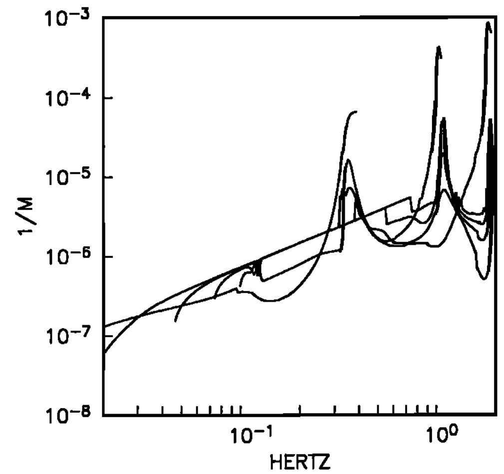

Fig. 15. The attenuation coefficient for Rayleigh waves in the model of figure 3.

ure 15. The coefficients lie mostly between 10^{-5} and 10^{-7} m^{-1} and the e-folding distances are between 100 and 10000 km. These are large distances but not large compared to the size of ocean basins. The seafloor microseism spectrum probably varies only slowly from location to location, since seismic waves from one location will propagate to other locations that are the order of a e-folding distance away. The spectral level will be much higher in unusual regions with large local forcing, like coastlines or under storms. Scattering of the seismic waves at changes in topography will reduce the distances microseisms travel.

CONCLUSIONS

We have tried to outline the causes of electric field and pressure fluctuations at the seafloor in a broad frequency band of interest to oceanographers and seismologists. We identify fluctuations in the pressure field at frequencies below 0.04 Hz as caused by long-period surface gravity waves. These waves deserve further study. The large energy associated with coastally trapped waves usually obscures the freely propagating waves of the open ocean in measurements made at the coastlines. The spectrum of these waves is expected to vary little from location to location or from season to season, but the validity of this prediction has not been verified.

The low noise level observed in the band between the gravity waves and the microseism peak provides an excellent opportunity for examining oceanic structure with seismic surface waves using seafloor stations. These frequencies between 0.025 and 0.1 Hz are appropriate for studying the lower crust and upper mantle.

The microseism peak has been repeatedly studied, but there has not been a study with sufficient oceanographic observations as well as seafloor seismic observations to determine the adequacy of the present theories of microseism generation. We unfortunately have had to rely on a modeling of the wind wave field rather than direct wave measurements, but the very good agreement between the shape of the observed spectral peaks and the predictions is encouraging.

Last, we have identified sharp peaks in the electric field spectrum at frequencies above a few tenths of a hertz with seismic waves trapped in the upper layers of the sediment. These waves are probably associated with the higher noise levels usually observed on the horizontal components of seafloor seismographs. This view is supported by observations from borehole seismographs. The noise level is much lower (28 dB at 2 Hz) in the borehole measurements and the horizontal and vertical noise levels in the borehole are comparable [*Adair et al.*, 1984].

Acknowledgments. We gratefully acknowledge helpful discussions with John Orcutt, Guy Masters, Joan Gomberg, and Alan Chave. We thank Tom Deaton, Steve Constable, Tim Field, Paul Fortuin, and John Lyons for their assistance during the development of the instruments. We commend the crew of the *Ellen B. Scripps* for their able support. This work was supported by the Office of Naval Research.

REFERENCES

Adair, R. G., J. A. Orcutt, and T. H. Jordan, Analysis of ambient seismic noise recorded by downhole and ocean bottom seismometers on the deep sea drilling project leg 78B, *Initial Rep. Deep Sea Drill. Proj.*, *78*, 767–781, 1984.

Agnew, D. C., and J. Berger, Vertical seismic noise at very low frequencies, *J. Geophys. Res.*, *83*, 5420–5424, 1978.

Aki, K., and P. G. Richards, *Quantitative Seismology, Theory and Methods*, vol. 1, W. H. Freeman, San Francisco, Calif., 1980.

Bradner, H., Probing sea-bottom sediments with microseismic noise, *J. Geophys. Res.*, *68*, 1788–1791, 1963.

Bradner, H., and J G. Dodds, Comparative seismic noise on the ocean bottom and on land, *J. Geophys. Res.*, *69*, 4339–4348, 1964.

Bradner, H , J. G. Dodds, and R. E. Foulks, Investigation of microseism sources with ocean bottom seismometers, *Geophysics*, *30*, 511–526, 1965

Brocher, T M., and B. T. Iwatake, Sources of low frequency ambient seafloor noise on the continental shelf, *Bull. Seismol. Soc. Am.*, *72*(4), 1129–1142, 1982.

Cox, C. S., J H. Filloux, and J. C. Larsen, Electromagnetic studies of ocean currents and electrical conductivity below the ocean floor, in *The Sea*, vol. 4, edited by A. E. Maxwell, pp. 637–693, John Wiley, New York, 1970.

Cox, C. S., N. Kroll, P. Pistek, and K. Watson, Electromagnetic fluctuations induced by wind waves on the deep seafloor, *J. Geophys. Res.*, *83*, 431–442, 1978.

Cox, C. S., T. Deaton, and S. C. Webb, A deep sea differential pressure gauge, *J. Atmos. Oceanic Technol.*, *1*(3), 237–246, 1984.

Filloux, J. H., Pressure fluctuations on the open ocean floor over a broad frequency range: New program and early results, *J. Phys. Oceanogr.*, *10*, 1959–1971, 1980.

Hasselmann, K. A., A statistical analysis of the generation of microseisms, *Rev. Geophys.*, *1*, 177–210, 1963.

Hasselmann, K. A., T. P. Barnett, E. Bouws, H. Carlson, P. E. Cartwright , K. Enke, J. A. Ewing, H. Gienapp, D. E. Hasselmann, P. Kruseman, A. Meerburg, P. Müller, D. J. Olbers, K. Richter, W. Sell, and H. Walden, Measurements of wind-driven growth and swell decay during the joint North Sea wave project (JONSWAP), Dtsch. Hydrogr. Inst., Hamburg, 1973.

Haubrich, R. A., The origin and characteristics of microseisms at frequencies below 140 cycles per hour, *Extrait Monogr. 31*, Union et Geophysique Internationale Symposium sur les Microseisms, Paris, 1970.

Haubrich, R. A., W. H. Munk, and F. E. Snodgrass, Comparative spectra of microseisms and swell, *Bull. Seismol. Soc. Am.*, *53*(1), 27–37, 1963.

Hughes, B., Estimates of underwater sound (and infra sound) produced by nonlinearly interacting ocean waves, *J. Acoust. Soc. Am.*, *60*(5), 1032–1039, 1976.

Kadota, T. T., and F. M. Labianca, Gravity wave induced pressure fluctuations in the deep ocean, *IEEE J. Oceanic Eng.*, *6*(2), 50–58, 1981.

Kibblewhite, A.C., and K.C. Ewans, Wave-wave interactions, microseisms and infrasonic ambient noise in the ocean, *J. Acoust. Soc. Am.*, *78*(3), 981–994, 1985.

Latham, G. V., and A. A. Nowroozi, Waves, weather and ocean bottom microseisms, *J. Geophys. Res.*, *73*, 3945–3956, 1968.

Latham, G. V., and G. H. Sutton, Seismic measurements on the ocean floor, *J. Geophys. Res.*, *71*, 2545–2573, 1966.

Latham, G. V., R. S. Anderson, and M. Ewing, Pressure variations produced at the ocean bottom by hurricanes, *J. Geophys. Res.*, *72*, 5693–5703, 1967.

LeBlond, P. H., and L. A. Mysak, *Waves in the Ocean*, Elsevier Scientific, Amsterdam, 1978.

Longuet-Higgins, M. S., A theory of the origin of microseisms, *Philos. Trans. R. Soc. London, Ser. A*, *243*, 1–35, 1950.

Longuet-Higgins, M. S., D. E. Cartwright, and N. D. Smith, Observations of the directional spectrum of sea waves using the motions of a floating buoy, in *Ocean Wave Spectra*, pp. 111–132, Prentice-Hall, Englewood Cliffs, N. J., 1963.

McGrath, J. R., Infrasonic seismic noise at the mid-Atlantic ridge near 37°N, *J. Acoust. Soc. Am.*, *60*(6), 1290–1299, 1976.

Munk, W. H., F. E. Snodgrass, and F. Gilbert, Long waves on the continental shelf: An experiment to separate trapped and leaky modes, *J. Fluid Mech.*, *20*(4), 529–554, 1964.

Nichols, R. H., Infrasonic ambient ocean noise measurements: Eleuthera, *J. Acoust. Soc. Am.*, *69*(4), 971–981, 1981.

Philips, O. M., *The Dynamics of the Upper Ocean*, 2nd ed., Cambridge University Press, New York, 1980.

Pierson, W. J., Jr., and L. Moskowitz, A proposed spectral form for fully developed wind seas based on the similarity theory of S. A. Kitaigorodskii, *J. Geophys. Res. 69*, 5181–5190, 1964.

Prothero, W., and W. H. Munk, Benthic array, final report: Advanced Research Projects Agency orders 1348 and 1809, *SIO ref. 74-24*, Scripps Inst. of Oceanogr., La Jolla, Calif., 1974.

Prothero, W. A., and W. Schaecher, First noise and teleseismic readings on a new ocean bottom seismometer capsule, *Bull. Seismol. Soc. Am.*, *74*(3), 1043–1058, 1984.

Snodgrass, F. E., G. W. Groves, K. F. Hasselmann, G. R. Miller, W. H. Munk, and W. H. Powers, Propagation of ocean swell across the Pacific, *Philos. Trans. R. Soc. London, Ser. A, 259*, 431–497, 1966.

Sorrells, G. G., and E. J. Douze, A preliminary report on the infrasonic waves as a source of long-period seismic waves, *J. Geophys. Res.*, *79*, 4908–4917, 1974.

Sorrells, G. G., and T. T. Goforth, Low frequency earth motion generated by slowly propagating partially organized pressure fields, *Bull. Seismol. Soc. Am.*, *63*(5), 1583–1601, 1973.

Spudich, P., and J. Orcutt, Petrology and porosity of an oceanic crustal site: Results from wave modeling of seismic refraction data, *J. Geophys. Res.*, *85*, 1409–1433, 1980.

Takeuchi, H., and M. Saito, Seismic surface waves, in *Seismology: Surface Waves and Earth Oscillations, Methods Comput. Phy.*, vol. 11, edited by B. A. Bolt, pp. 217–295, Academic, Orlando, Fla., 1972.

Tyler, G. L., C. C. Teague, R. H. Stewart, A. M. Peterson, W. H. Munk, and J. W. Joy, Wave directional spectra from synthetic aperture observations of radio scatter, *Deep Sea Res.*, *21*, 989–1016, 1974.

Webb, S. C., Observations of Seafloor pressure and electric field fluctuations, Ph.D. Thesis, UCSD, 1984.

Webb, S. C., and C. S. Cox, Electromagnetic fields induced at the seafloor by Rayleigh-Stoneley waves, *J. Geophys. Res.*, *87*, 4093–4102, 1982.

Webb, S., and C.S. Cox, Pressure and electric fields on the deep seafloor: Background noise for seismic detection, *Geophys. Res. Lett.*, *11*(10), 967–970, 1984.

Wiechert, E., Verhandlungen der Zweiten Internationalen Seismologischen Konferenz, *Gerlands Beitr. Geophys., Ergänzungsbd. 2*, 41–43, 1904.

Wimbush, M., and W. Munk, The benthic boundary layer, in *The Sea*, vol. 4, edited by A. E. Maxwell, pp. 731–758, John Wiley, New York, 1970.

C. S. Cox, Scripps Institution of Oceanography, UCSD, A-030, La Jolla, CA 92093.

S. C. Webb, Woods Hole Oceanographic Institution, Woods Hole, MA 02543.

(Received March 21, 1985;
revised January 21, 1986;
accepted January 24, 1986.)